A Prescribed-Wake Vortex Lattice Method for Preliminary Design of Co-Axial, Dual-Rotor Wind Turbines

Aaron Rosenberg
Graduate Student, Student Member of ASME
Department of Aerospace Engineering
Iowa State University
Ames, Iowa 50011
Email: aaronr@iastate.edu

Anupam Sharma*
Assistant Professor, Member of ASME
Department of Aerospace Engineering
Iowa State University
Ames, Iowa 50011
Email: sharma@iastate.edu

ABSTRACT

This paper extends the prescribed wake vortex lattice method (VLM) to perform aerodynamic analysis of dual-rotor wind turbines (DRWTs). A DRWT turbine consists of a large, primary rotor placed co-axially behind a smaller, secondary rotor. The additional vortex system introduced by the secondary rotor of a DRWT is modeled while taking into account the singularities that can occur when the trailing vortices from the secondary (upstream) rotor interact with the bound vortices of the main (downstream) rotor. Pseudo-steady assumption is invoked and averaging over multiple relative rotor positions is performed to account for the primary and secondary rotors operating at different rotational velocities. The VLM solver is first validated against experiments and blade element momentum theory results for a conventional, single rotor turbine. The solver is then verified for two DRWT designs against results from two CFD methods: (1) Reynolds Averaged Navier-Stokes CFD with an actuator disk representation of the turbine rotors, and (2) Large Eddy Simulations with an actuator line model. Radial distributions of sectional torque force and angle of attack show reasonable agreement between the three methods. Results of parametric sweeps performed using VLM agree qualitatively with RANS CFD results demonstrating that the proposed VLM can be used to guide preliminary design of DRWTs.

*Corresponding author

Nomenclature

A $= \pi r_t^2$, area swept by the rotor
P aerodynamic power extracted by a turbine
T aerodynamic thrust (force) exerted on the turbine along the wind direction
Q $= 0.5(\Omega_{ij}\Omega_{ji} - S_{ij}S_{ji})$, where Ω_{ij} and S_{ij} are rotation- and strain rate tensors respectively
C_P $= 2P/(\rho u_\infty^3 A)$, aerodynamic power coeff. of a turbine
C_T $= 2T/(\rho u_\infty^2 A)$, aerodynamic thrust coeff. of a turbine
$\overline{Z}$ time average of variable Z
Z' $= Z - \overline{Z}$, temporal fluctuation of variable Z
$\widetilde{Z}$ spatially filtered value of variable Z
$\langle Z \rangle$ horizontally averaged value of variable Z
a $= 1 - u/u_\infty$, axial induction factor
a_w axial induction in the turbine wake
c_T section thrust force coefficient
c_d section drag force coefficient
c_l section lift force coefficient
c_{τ_F} section torque force coefficient
f_i force per unit volume exerted by turbine rotor on the flow
g_0 gravitational acceleration on Earth
k $= 0.5\,\overline{u_i' u_i'}$, turbulent kinetic energy
p pressure
p^* $= \widetilde{p}/\rho_0 + \widetilde{u_i}\widetilde{u_j}/2$, modified kinematic pressure
q_j $= \widetilde{u_j\theta} - \widetilde{u_j}\widetilde{\theta}$, sub-grid or (sub-filter) scale heat flux
r_t rotor tip radius
u_i local velocity vector
u_∞ freestream wind speed
Γ $= \oint u_i \, \mathrm{d}s_i$, circulation
Δ $=(\Delta_x\Delta_y\Delta_z)^{1/3}$, cube-root of cell volume
$\Delta_x, \Delta_y, \Delta_z$ cell size in each coordinate direction
Ω angular velocity of turbine rotor
α thermal diffusivity of air in Eq. 5; angle of attack elsewhere
δ_{ij} Kronecker delta; $\delta_{ij} = 1$ for $i = j$; 0 for $i \neq j$
θ_0 reference potential temperature
ε turbulent dissipation
θ potential temperature
λ $= \Omega r_t/u_\infty$, tip speed ratio
ν kinematic viscosity of air
ρ_0 reference (freestream) air density
τ_{ij} $= \widetilde{u_i u_j} - \widetilde{u_i}\widetilde{u_j}$, sub-grid (or sub-filter) scale stress tensor
ϕ angle between blade-relative velocity and plane of rotor rotation

Subscripts

$(\,)_{,eq}$ a qty. defined for DRWT in a manner equivalent to SRWT
$(\,)_s$ or $(\,)_{,s}$ related to the secondary rotor of a DRWT
$(\,)_m$ or $(\,)_{,m}$ related to the main rotor of a DRWT

1 Introduction

Dual-rotor wind turbine (DRWT) technology (see Fig. 1) has recently been investigated [1–5] as a higher efficiency alternative to conventional, single-rotor wind turbines (SRWTs). The technology uses two coaxial rotors to harness energy from wind. The two rotors can have different or same diameters, and can rotate with the same rotational speed (e.g., if they are on the same shaft) or independent of each other. DRWTs have additional parameters compared to SRWTs, such as relative rotor sizes, rotation speeds, axial separation, etc. These parameters must be carefully selected to optimize the aerodynamic performance of a DRWT. Due to the large parametric space that needs to be explored, it is desirable to have a computationally inexpensive analysis method to provide preliminary design guidance.

Blade element momentum (BEM) theory based methods and vortex lattice/line methods have been used extensively in design and analysis of SRWTs. These methods have been modified to investigate DRWTs. Lee *et al.* [6] uses a modified BEM method to study the effects of design parameters on a counter-rotating wind turbine. This method assumes that second rotor operates completely inside the developed wake of the primary (main) rotor. Jung *et al.* [4] also uses a modified BEM method in which the wake from the front rotor is prescribed using experimental data. This allows for the second rotor to operate in the partial wake of the front rotor. A free-wake vortex lattice method has also been used successfully to study multi-rotor wind turbines [7, 8]. This has proven to be a relatively high fidelity method for simulating multi-rotor wind turbines, but it can be computationally expensive especially for design use where a large parametric space is required to be explored.

In this paper, we present a methodology to extend the prescribed-wake vortex lattice method to carry out preliminary aerodynamic analysis of DRWTs. This proposed method allows for a general analysis of DRWTs at a relatively low computational cost.

2 Vortex Lattice Method

The vortex lattice method is based on Prandtl's lifting line theory, which utilizes the laws of kinematics (Helmholtz vortex theorems) and dynamics (Kelvin's circulation theorem) of vortex lines. Potential flow is assumed and rotor blades are replaced by blade-bound vorticity (lifting lines). The bound vorticity for a blade section (airfoil) can be concentrated at a point or distributed along the airfoil chord/camber line; vorticity and circulation are related by Stokes' theorem. Helmholtz vortex theorems necessitate the existence of a single free-trailing vortex sheet per blade. They also define the distribution of the trailing vorticity; the strength of each trailing vortex is equal to the change in circulation along the lifting line.

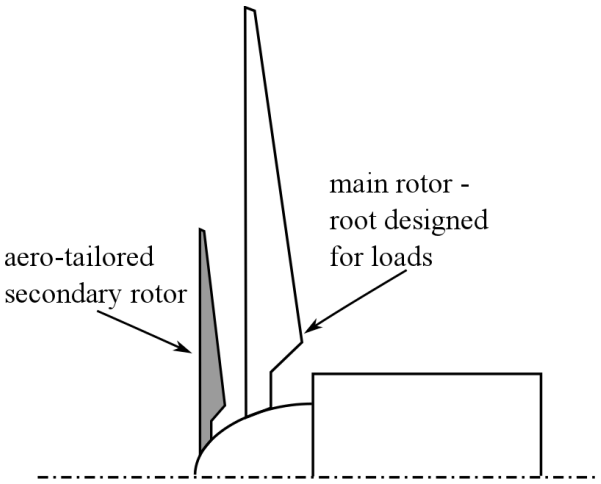

Fig. 1: A schematic of the DRWT technology by Rosenberg *et al.* [1]

Velocity "induced" by vorticity is described by the Biot-Savart law. In an aircraft, the velocity induced on the wing by the trailing vortex sheet is referred to as "downwash". This downwash is responsible for induced drag in finite-span wings. The same concept can be applied to wind turbine rotor blades (or propeller blades), where the trailing vortex sheet becomes helical due to blade rotation. Induction determines the local flow velocity and, given blade geometry and operation specifications, the local blade-relative flow velocity and angle of attack. With prior knowledge of sectional lift and drag polars ($c_l - \alpha$ and $c_d - \alpha$ curves), the local lift and drag can be computed. Finally, the Kutta-Jukowski theorem links the sectional lift to the bound

circulation around a blade section. Using these theorems, an iterative procedure can be obtained to compute spanwise distribution of circulation (or blade-bound vorticity) on turbine rotor blades (see e.g., Refs. [9, 10]).

Based on the treatment of trailing vorticity, the vortex lattice method can be classified as either *free wake* or *prescribed (fixed) wake* [11]. In the free-wake approach, mutual induction between trailing vortex elements is permitted and hence the wake evolves with time; the wake structure can deform substantially over time. In the prescribed-wake approach, mutual induction is ignored and the prescribed trailing vortex structure stays intact. Subtle changes to the wake structure that do not change the wake helix topology, such as the helix pitch, Trefftz plane location, etc. are permitted in the prescribed-wake approach until convergence is reached. These changes are specified as functions of some overall integrated quantity such as rotor thrust or power coefficient.

While the free-wake approach is of higher fidelity, it is computationally expensive [11] and can suffer from robustness issues. The prescribed-wake approach, on the other hand, is relatively quick and robust, but can be inaccurate if the fixed wake structure is poorly specified. We choose the prescribed-wake approach here as the objective is to explore a large design space during preliminary design of DRWTs. For our purpose, efficiency and robustness are more important than fidelity as long as the methodology predicts correct design trends. The particular implementation presented in Refs. [10, 12, 13] is adopted in our prescribed-wake vortex lattice method solver with two major changes that are described below.

Chattot [13] assumes 'wake equilibrium' to relate computed turbine power coefficient, C_P with that given by the 1-D momentum theory to obtain axial induction factor, a using the relation $C_P = 4a(1-a)^2$. This axial induction factor is then used to update the pitch of the trailing vortex helix in an iterative procedure until convergence is achieved. The problem with this approach is that axial induction is a multi-valued function of C_P (see Fig. 2). Typically, the solution corresponding to smaller axial induction factor is selected to set the helix pitch. While this strategy works for low-loading conditions, it is evident from Fig. 2 that this approach is incorrect for cases with high rotor disk loading. An alternative is to choose the turbine thrust force coefficient, C_T to calculate a. However, if the 1-D momentum theory formula for C_T is chosen (i.e., $C_T = 4a(1-a)$), then the non-uniqueness problem still persists (see Fig. 2) although the range of application is increased to $0 < a < 0.5$. We get around this non-uniqueness problem by using the empirical formula for C_T by Buhl [14] which incorporates corrections for high disk (rotor) loading. The formula (Eq. 1, with $F = 0.9$) provides a one-to-one mapping between a and C_T as can be seen in Fig. 2.

$$C_T(a) = \begin{cases} 4aF(1-a) & \text{if } 0 \le a \le 0.4 \\ \dfrac{8}{9} + \left(4F - \dfrac{40}{9}\right)a + \left(\dfrac{50}{9} - 4F\right)a^2 & \text{if } 0.4 < a \le 1 \end{cases} \tag{1}$$

The second major change from Chattot's implementation [13] is in prescribing turbine wake structure. The wake behind a turbine expands and its convection velocity reduces from the rotor plane to the Trefftz plane. In previous works [10, 12, 13], the Trefftz plane was assumed to be located at the axial location where the wake completes three rotor revolutions, making it dependent on the tip speed ratio. The local axial induction, $a_w(x)$ was assumed to vary linearly with downstream distance between the rotor plane and the Trefftz plane. We conducted a number of CFD runs varying rotor tip speed ratio (to vary rotor thrust) to understand the wake structure behind a wind turbine. The CFD methodology is described later in Section 3.1.1. Based on the CFD results we find that: (1) axial induction does not vary linearly with downstream distance, (2) it correlates well with thrust coefficient, C_T and (3) is independent of tip speed ratio when scaled appropriately. A reasonable collapse for a wide range of data

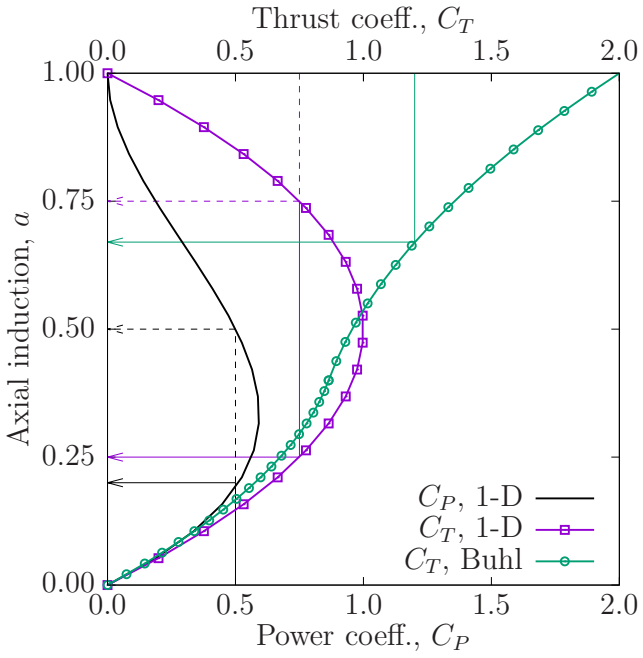

Fig. 2: Functions to obtain axial induction factor, a from C_P and C_T given by 1-D momentum theory, and from C_T given by Eq. 1.

is obtained with the correlation -

$$\frac{a_w(x)}{a} = 1.85 - 0.85 \exp\left(-\frac{2}{3\sqrt{C_T}} \times \frac{x}{r_t}\right), \tag{2}$$

where r_t is the rotor tip radius and $a_w(x)$ is the area-averaged axial induction in the rotor wake at a distance x from the rotor plane; $a = a_w(0)$ is the induction at the rotor plane. Equation 2 and Fig. 3 suggest

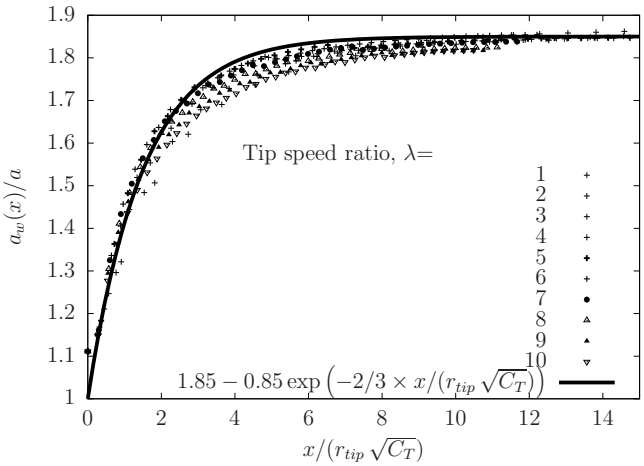

Fig. 3: A correlation derived using wake data from a number of RANS CFD simulations.

that the axial induction goes only up to $1.85 \times a_w(0)$ at the Trefftz plane. Note that the 1-D momentum theory requires the axial induction to reach $2 \times a_w(0)$ at the Trefftz plane. This difference in CFD is

likely due to diffusion of the wake with the freestream, which is physical. Numerical dissipation in CFD can also be the cause; the authors have performed a grid independence study [15] to rule out the grid resolution issue. We use Eq. 2 to prescribe the wake structure in our VLM implementation as opposed to the linear variation used in earlier works. Also, the wake expands radially as it convects downstream. The radial expansion is determined using mass conservation as $r(x) = r(0) \times \sqrt{(1-a)/(1-a_w(x))}$. The following section summarizes the prescribed-wake VLM algorithm for conventional, single-rotor turbines with the proposed changes.

2.1 Algorithm

Turbine information such as turbine rotor size, airfoil polars etc. are first read from user-specified input files. A value of C_T is assumed to compute the induction at the rotor plane, a. Equation 2 then gives the distribution of axial induction $a_w(x)$, which along with the rotor tip speed ratio defines the initial wake helix structure. Induction coefficients for each point in the wake helix at each point on the blade are computed and stored. Since these coefficients only depend on the geometry, they stay constant as long as the wake helix shape remains the same.

An initial approximation of the blade bound circulation, Γ is computed using the Kutta-Jukowski theorem while assuming the local induction at the rotor plane to be a (computed earlier). Given the Γ distribution along the blade, the strengths of the trailing vortices at each radial location is determined by conserving circulation. Induction, and consequently the angle of attack at each radial location on the blade, are then calculated using the pre-computed induction coefficients. Airfoil polars then give the sectional lift and drag forces which are decomposed into the rotor-plane and out-of-rotor-plane components and integrated over the entire blade span to get the turbine thrust force and power coefficients. The Kutta-Jukowski theorem then gives a new approximation of sectional circulation, Γ_{new}. Iterations on Γ are performed with a fixed wake helix until it converges to within a specified tolerance. A new value of a is computed with the relation given in Eq. 1 using the last-computed value of C_T. The pitch of the wake helix is adjusted using Eq. 2 and the entire process is repeated until C_P converges.

2.2 Validation

Our implementation of the vortex lattice method, with the proposed modifications, is validated against experimental data and blade element momentum (BEM) theory predictions. The three-bladed, stall controlled, 95 kW Tellus T-1995 wind turbine is used for validation (measurement data from Ref. [16]). In the report [16], this turbine is referred to as Risø turbine. The turbine rotor diameter is 19 m. The turbine rotor blade chord and twist distributions are plotted in Fig. 4. Other details about the turbine, such as the airfoils used along the span, and the lift and drag polars are available in Ref. [16].

Figure 5 (a) compares turbine power variation with wind speed as predicted by the prescribed wake vortex lattice method solver against measured data as well as BEM theory predictions. The agreement with data by both prediction methods is good in the low-speed range, with the VLM showing a slightly better agreement. As the wind speed increases beyond about 12 m/s, the turbine starts to stall and 3D, spanwise flow becomes increasingly important. It is well known that such spanwise flow alleviates stall in 3D blades and allows them to operate at higher angles of attack than a corresponding 2-D airfoil. This 3D flow effect cannot be captured by strip-theory based methods such as the VLM and BEM. Therefore, the predictions fall short of the experimentally-measured turbine power in the region marked as "3-D stall effects" in the figure. Figure 5 (b) plots the same data as in Fig. 5 (a), but in the form of characteristic $C_P - \lambda$ curves, where λ is the rotor tip speed ratio. The agreement with data is good outside the stall region.

Code-to-code comparisons (between vortex lattice method and BEM) of spanwise variations of sec-

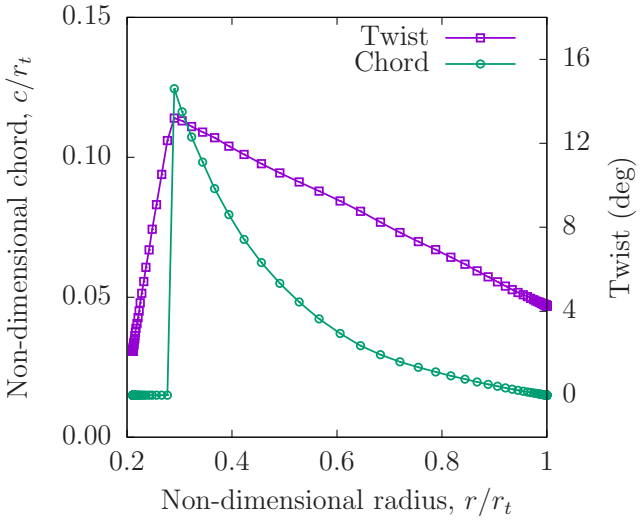

Fig. 4: Non-dimensional chord and twist distributions for the model Tellus T-1995 (Risø) turbine used for validation [16]).

tional torque force coefficient, $c_{\tau F}$ and sectional thrust force coefficient, c_T are presented at the tip speed ratio, $\lambda = 6.0$ in Fig. 6. These coefficients are defined as

$$c_{\tau F} = c_l \sin(\phi) - c_d \cos(\phi), \text{ and}$$
$$c_T = c_l \cos(\phi) + c_d \sin(\phi),$$

where ϕ is the angle that the local blade-relative velocity vector makes with the plane of rotation, and c_l and c_d are the blade section lift and drag coefficients. The agreement between the two methods is very good. This verifies the solver capability for single rotor wind turbines. In the following section we present our approach to extend the vortex lattice method to DRWTs.

3 Extension to Dual-Rotor Wind Turbines

Several aspects need to be considered when evaluating the aerodynamic performance of dual-rotor wind turbines using a vortex lattice method:

1. Both rotors have trailing vortex sheets which have to be accounted for when calculating induction using the Biot-Savart law. Also, blade bound vorticity on the rotors mutually influence the induction on each other.
2. If the two rotors rotate independently, then the problem becomes inherently unsteady. Approximations need to be made to solve it as a steady problem.
3. If the two rotors are physically very close to each other then potential flow effects due to finite blade thickness also come into play.

To account for the mutual induction between the bound and trailing vortices of the two rotors of a DRWT, the associated vortex lattices need to be established. Figure 7 shows the vortex lattice structure of a DRWT. Two sets of helices are now present; one set each for the two rotors. The fact that the trailing vortices of both rotors are convected by the same flow speed is used to determine the pitches of the two helices. Equation 1 is used to determine the area-average induction at the rotor plane (a), and Eq. 2 to determine the variation of area-average induction with downstream distance ($a_w(x)$). Rotor

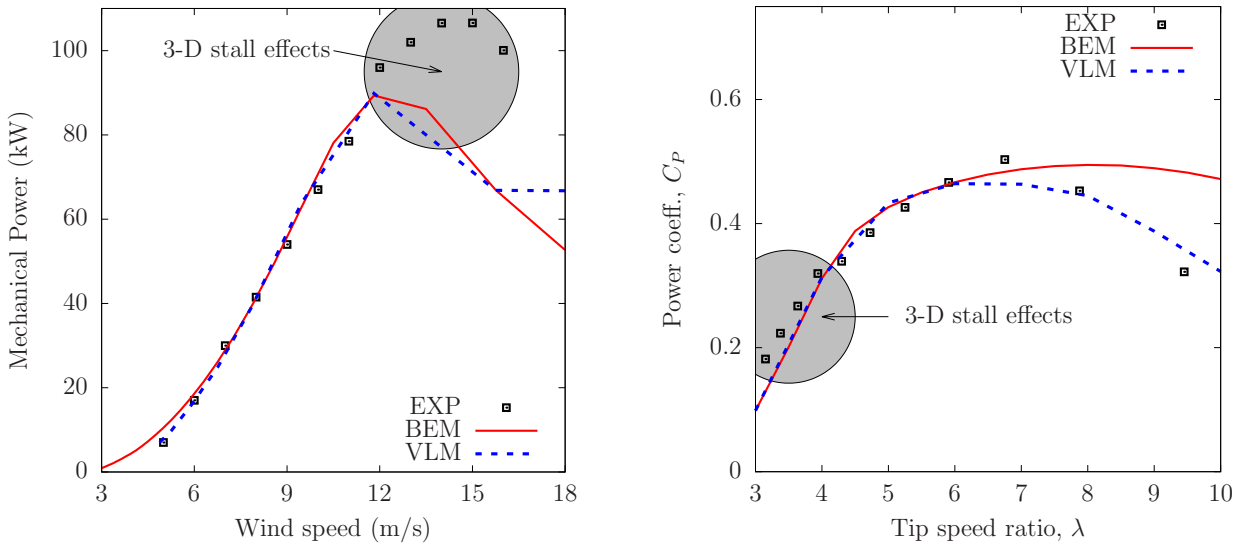

(a) Power versus speed

(b) $C_P - \lambda$

Fig. 5: Comparisons with experimental data and BEM results for the Tellus T-1995 (Risø) turbine: (a) power variation with wind speed, and (b) the same information presented as characteristic ($C_P - \lambda$) curves.

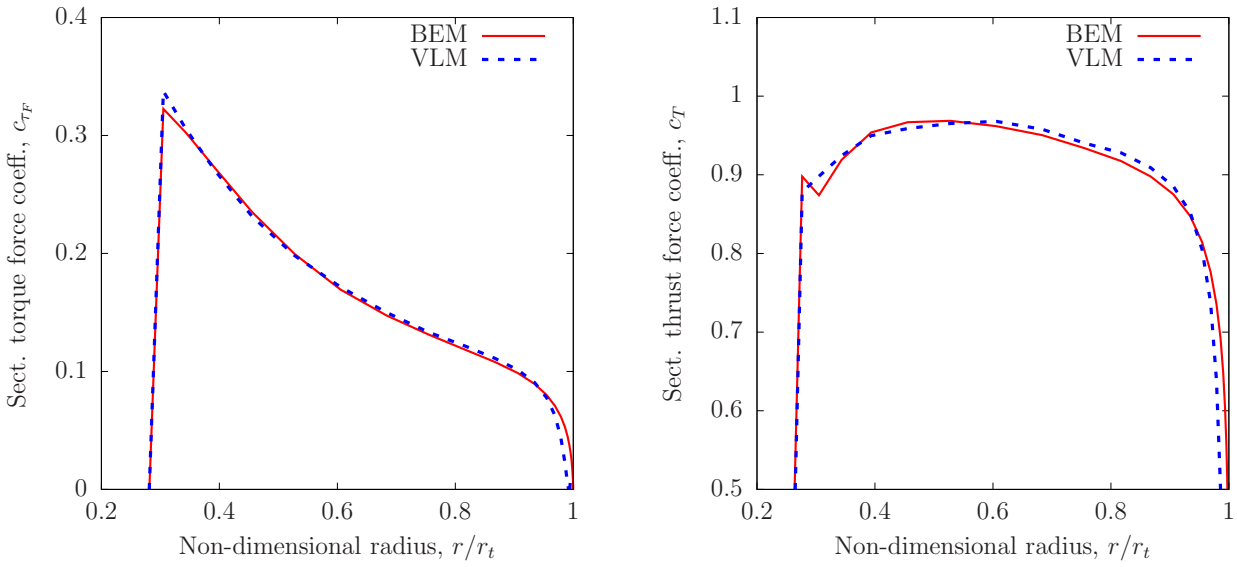

(a) sectional torque force coeff., c_{τ_F}

(b) sectional thrust force coeff., c_T

Fig. 6: Comparisons of radial variation of force coefficients at $\lambda = 6.0$ against BEM results for the Tellus T-1995 (Risø) turbine

tip speed ratio and $a_w(x)$ then determine the pitches of the wake helices. For DRWTs, an equivalent area-weighted $C_{T,eq}$ is used in place of C_T in Eqs. 1 and 2, where

$$C_{T,eq} = C_{T,m} + \frac{A_s}{A_m} C_{T,s}, \tag{3}$$

and subscripts 'm' and 's' refer to the main rotor and the secondary rotor respectively; 'A' is area of rotor disk. Similarly, aerodynamic power coefficient of a DRWT is defined as $C_{P,eq} = C_{P,m} + A_s/A_m\, C_{P,s}$, which is the ratio of power extracted by the turbine to the power in the air stream flowing through the turbine rotors. Once the vorticity structure is set, the computation of induction coefficients using the Biot-Savart law is straightforward. It should be emphasized again that the induction from blade bound vorticity of both the rotors has to computed and added to the induction computed using the trailing vorticity. Another complexity can arise in computing induction. A singularity arises if any point on

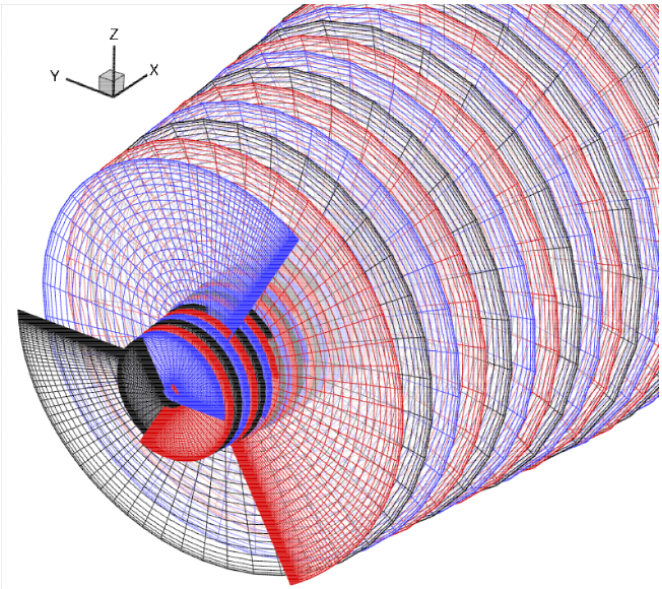

Fig. 7: Trailing wake vorticity behind the two rotors of a dual-rotor wind turbine. Each rotor is three bladed. The three colors: red, blue, and black denote the trailing vorticity from each blade of the two rotors.

the trailing vortex structure of the upstream rotor coincides with a point on a blade of the downstream rotor where induction is computed. This singularity is averted by imposing a minimum threshold on the distance between two such points - avoiding division by zero when applying the Biot-Savart law.

If the two rotors rotate independently, the problem becomes unsteady even if uniform inflow is assumed. This is because of the relative rotation of the two rotors and the resulting temporal variation of blade aerodynamics. Unsteady computations, even with a vortex lattice method are expensive and not very suitable for preliminary design. We therefore use a pseudo-steady approximation, wherein we compute turbine performance for different relative clock (angular) positions of the two rotors. Averaging over such steady solutions gives the net performance of a DRWT. Figure 8 plots the variation in $\%C_P$ of a DRWT for twelve relative rotor clock positions. The pattern repeats after 120^0 due to the periodicity in the problem; both rotors are three bladed. The maximum variation is observed to be less than 0.5%. For production runs, averaging is performed over five clock positions.

Potential effects due to blade thickness decay exponentially away from the blade surfaces. To illustrate this, Fig. 9 presents potential flow results using a vortex panel code for the NACA 0030 airfoil. NACA 0030 is a 30% thick airfoil, which is representative of the thickness of airfoils used in the blade root region of utility scale wind turbines. The flow Mach number is 0.2 and the angle of attack is 0 degrees. The contour plot in Fig. 9 (a) shows rapid convergence to freestream pressure away from the airfoil. Percentage difference between local and freestream values of flow speed and pressure are plotted with distance away from the airfoil in the upstream direction in Fig. 9 (b). The differences between local

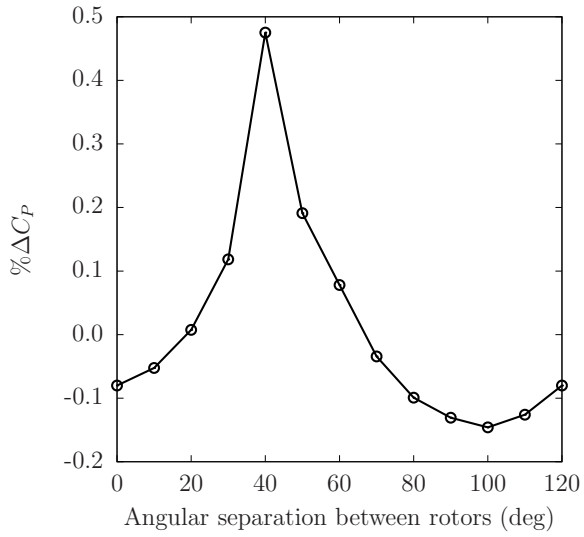

Fig. 8: Predicted variation in % C_P of a DRWT with relative angular position between the primary and the secondary rotors.

and freestream flow speed and pressure are less that 1.5% and 0.08% respectively. In the present approach, we neglect potential interaction between the rotors due to blade thickness by assuming that the axial separation between the rotors is greater than the rotor blade chord. Rosenberg *et al.* [1] suggests that the optimum axial separation for enhanced isolated rotor aerodynamic performance is about 0.2 $\times$ the main rotor diameter, which is much greater than the maximum blade chord of the main rotor. Thus, the approximation to neglect potential effects due to blade thickness should be valid for such turbines.

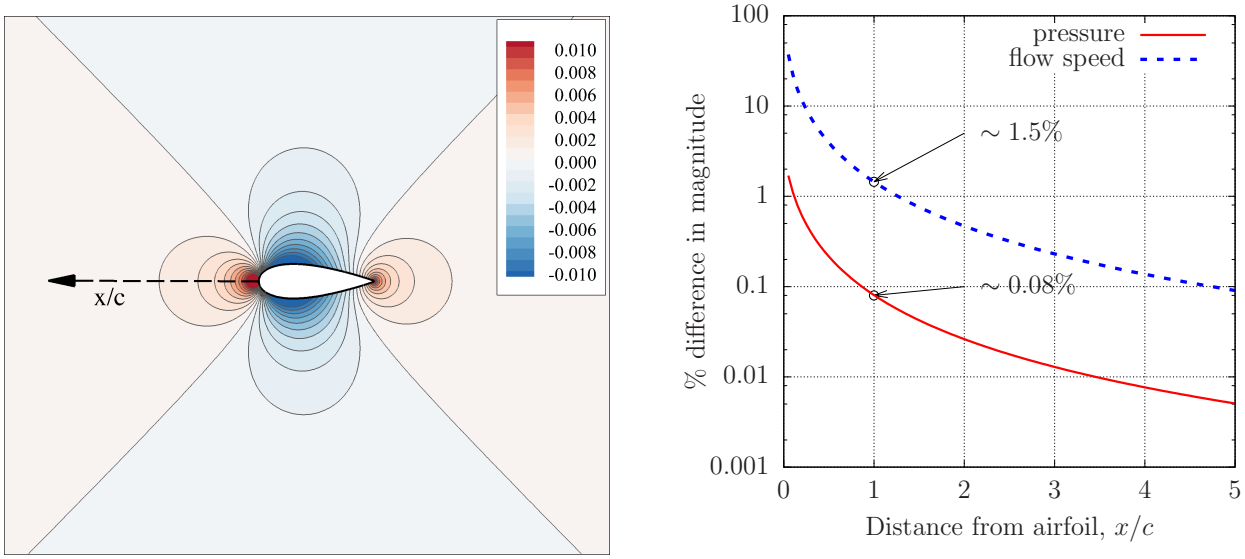

(a) contours of $\%\Delta p = 100 \times (p - p_\infty)/p_\infty$

(b) variation with distance from the airfoil

Fig. 9: Panel code results for the NACA 0030 airfoil at freestream Mach number of 0.2 and zero angle of attack: (a) contours of percentage difference between local and freestream pressure, and (b) magnitude of difference between local and freestream pressure and flow speed along the dashed line in (a).

The assumptions made in the proposed vortex lattice method for analysis of DRWTs are summarized below:

1. Potential interaction between the rotors due to blade thickness is neglected. This is justified for DRWTs where rotor-rotor separation is greater than blade chord.
2. Unsteadiness due to relative motion between the two rotors is not modeled. To get the net (time-averaged) effect, pseudo-steady, prescribed-wake VLM calculations are performed for multiple relative rotor clock positions and averaged. This assumption is verified in Section 3.1.3 by comparing VLM predictions against results from time-resolved CFD computations.

3.1 Verification with CFD

The proposed extended vortex lattice method to analyze dual-rotor wind turbines is verified against results obtained using two CFD methods: (1) the Reynolds Averaged Navier-Stokes + actuator disk (RANS/AD) method described in Selvaraj [17], and (2) the large eddy simulation + actuator line method (LES/ALM) method described in Ref. [18]. Subtle aspects of these two methods are summarized here for completeness.

3.1.1 RANS/AD Method

The RANS/AD method [1, 17] solves the incompressible RANS equations (Eq. 4) with the rotor blades modeled as body forces (actuator disk). The governing equations are

$$\begin{aligned} &\frac{\partial \bar{u}_i}{\partial x_i} = 0, \text{ and,} \\ &\bar{u}_j \frac{\partial \bar{u}_i}{\partial x_j} = -\frac{1}{\rho_0}\frac{\partial \bar{p}}{\partial x_i} + \nu \frac{\partial^2 \bar{u}_i}{\partial {x_j}^2} - \frac{\partial \overline{u_i' u_j'}}{\partial x_j} + \frac{f_i}{\rho_0}. \end{aligned} \tag{4}$$

In the above, the overbar denotes time averaging. The Reynolds stress tensor, $\overline{u_i' u_j'}$ is modeled using the standard two equation, $k-\varepsilon$ turbulence model [19]. The term f_i represents the body force per unit volume and is computed using the user-prescribed airfoil polars, and the local flow velocity. The body force, f_i is spatially distributed - the distribution takes a Gaussian shape along the flow direction and uniform along the radial direction. Linear interpolation is used to compute f_i at the computational grid points. Axisymmetric flow assumption is made to reduce the problem to two dimensions.

This RANS/AD model is implemented in OpenFOAM and has been validated against experimental data as well as Blade Element Momentum (BEM) theory solutions for single-rotor turbines [1, 17, 20]. Recently, we have improved this methodology by incorporating Prandtl's tip loss correction following Mikkelsen [21]. The RANS/AD results presented in this paper use this improved model and are therefore slightly different from those in Refs. [17, 20].

The use of the RANS/AD CFD method to analyze DRWTs is described in Ref. [1]. Figure 10 shows an example computational grid and a CFD solution for flow over a DRWT. In this example the secondary rotor tip radius is 0.4 times that of the main rotor, and the main and secondary rotors are placed at $x = +0.1$ and $x = -0.1$ respectively. The physical coordinates are nondimensionalized by the rotor tip radius, r_t.

3.1.2 LES/ALM Method

The LES/ALM model implementation in the Simulator fOr Wind Farm Application (SOWFA) [18] software is used here. In this model, spatially filtered, incompressible forms of continuity and Navier-Stokes equations are solved using spatial and temporal discretization, and the actuator line model (ALM)

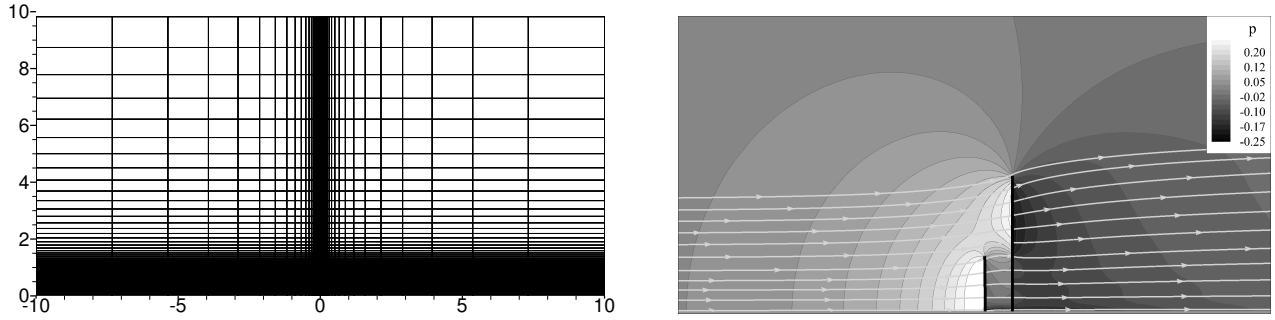

(a) Grid (b) Solution (zoom view)

Fig. 10: Computational grid and result of the RANS/AD method applied to a DRWT: (a) axisymmetric grid (every fifth point shown for clarity), and (b) pressure contours and streamlines (zoomed in near the DRWT).

is used for rotor parameterization. Spatial filtering introduces unresolved, sub-grid scale (SGS) stresses, which have to be modeled. The width of the spatial filter is taken to be the grid-filter width given by $\Delta = (\Delta_x \Delta_y \Delta_z)^{1/3}$. Denoting spatially-filtered quantities by $\widetilde{(\cdot)}$, the governing fluid flow equations are

$$\begin{aligned}
\frac{\partial \widetilde{u_i}}{\partial x_i} &= 0, \\
\frac{\partial \widetilde{u_i}}{\partial t} + \widetilde{u_j}\left(\frac{\partial \widetilde{u_i}}{\partial x_j} - \frac{\partial \widetilde{u_j}}{\partial x_i}\right) &= -\frac{\partial \widetilde{p^*}}{\partial x_i} - \frac{\partial \tau_{ij}}{\partial x_j} + \nu \frac{\partial^2 \widetilde{u_i}}{\partial x_j^2} - \underbrace{f_i/\rho_0}_{\text{blade force}} + \underbrace{\delta_{i3} g_0 (\widetilde{\theta} - \langle \widetilde{\theta} \rangle)/\theta_0}_{\text{buoyancy force}}, \\
\frac{\partial \widetilde{\theta}}{\partial t} + \widetilde{u_j}\frac{\partial \widetilde{\theta}}{\partial x_j} &= -\frac{\partial q_j}{\partial x_j} + \alpha \frac{\partial^2 \widetilde{\theta}}{\partial x_j^2},
\end{aligned} \tag{5}$$

where, $\widetilde{p^*} = \widetilde{p}/\rho_0 + \widetilde{u_j}\widetilde{u_j}/2$ is the modified kinematic pressure, $\tau_{ij} = \widetilde{u_i u_j} - \widetilde{u_i}\widetilde{u_j}$, is sub-grid scale (SGS) stress tensor, and $q_j = \widetilde{u_j \theta} - \widetilde{u_j}\widetilde{\theta}$ is SGS heat flux. θ is potential temperature, α is thermal diffusivity of the fluid, and f_i is a momentum source term that models the force exerted by turbine rotor blades. The DRWT is modeled in SOWFA by simulating the two rotors of the DRWT as two separate single-rotor turbines placed in tandem without the towers. The use of SOWFA to model DRWTs is described in Ref. [2]. Figure 11 shows a sample results from a DRWT simulation using SOWFA.

3.1.3 Code-to-Code Comparisons

Two DRWT configurations are chosen for code-to-code comparisons between results from the proposed VLM and the two CFD methods. The radius of the secondary rotor is selected to be 25% and 40% of the main rotor radius for the two designs, i.e., $r_{t,s}/r_{t,m} = 0.25$ and 0.4. However, both the DRWT configurations use the same *non-dimensional* rotors for the main rotor as well as the secondary rotor.

Figures 12 and 13 compare spanwise variations of local angle of attack and sectional torque force coefficients. The LES/ALM results are averaged over time and over the three blades of each rotor to generate the profiles; VLM results are phase averaged as described in Sec. 3. Good agreement between the results from the proposed VLM and the two CFD methods is observed for both the primary and the secondary rotors for the two DRWTs. The differences are largest at the radial location corresponding to the tip radius of the secondary rotor. This is expected for two reasons: (1) the turbulence in the CFD simulations (both RANS and LES) will diffuse the trailing vortex sheet of the secondary rotor while the VLM has no such mechanism, and (2) the RANS/AD model smears the effect of individual blades over

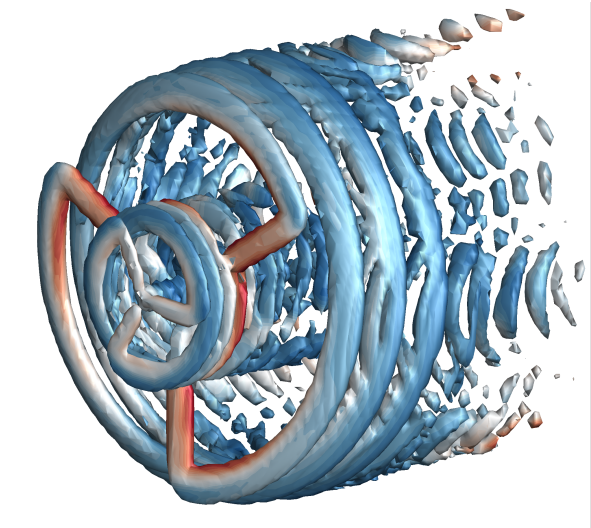

Fig. 11: Iso-surfaces of Q-criterion ($Q = 0.05$) computed using the LES/ALM method. The surfaces show the bound and trailing vortices and are colored with the r.m.s. of axial velocity.

the entire disk, whereas the VLM models each individual blade trailing vorticity independently. Even though VLM results are averaged over multiple relative clock positions of the two rotors in the proposed algorithm, it should be realized that this averaging is not the same as azimuthally averaging the trailing vortices, which is what happens in the RANS/AD method.

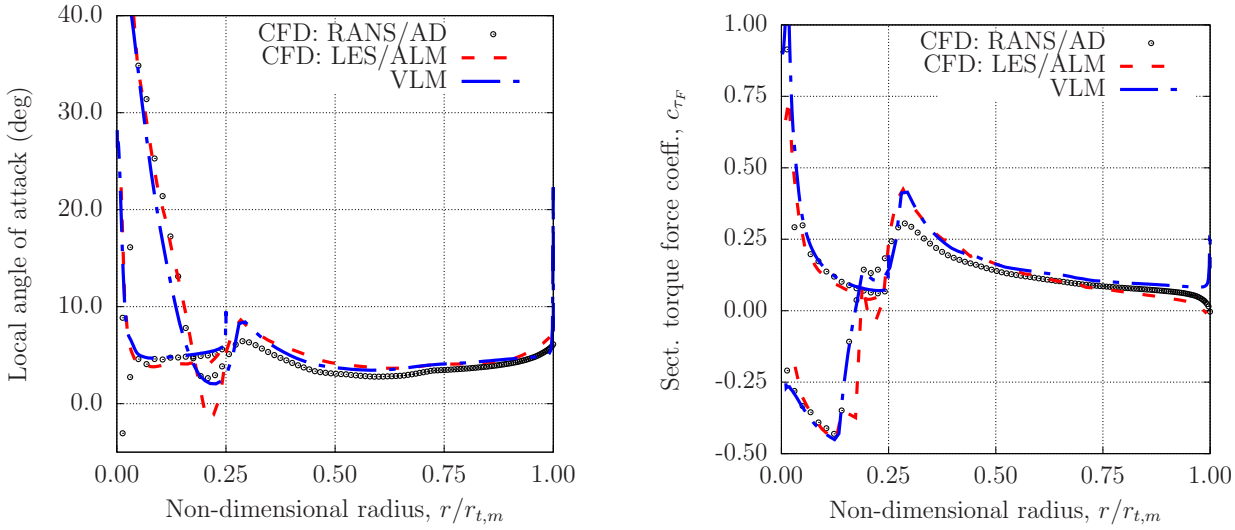

(a) angle of attack, α

(b) sectional torque force coeff., $c_{\tau F}$

Fig. 12: Comparisons between CFD and VLM of spanwise variations of angle of attack and torque force coefficient for the following parameters of the secondary rotor: $r_{t,s}/r_{t,m} = 0.25$ and $\lambda_s = 8.0$.

4 Preliminary Design of a Dual-Rotor Wind Turbine

The proposed vortex lattice method is used to perform parametric sweeps for a DRWT design. One such study using the RANS/AD method was presented in Ref. [1] where the secondary rotor diameter,

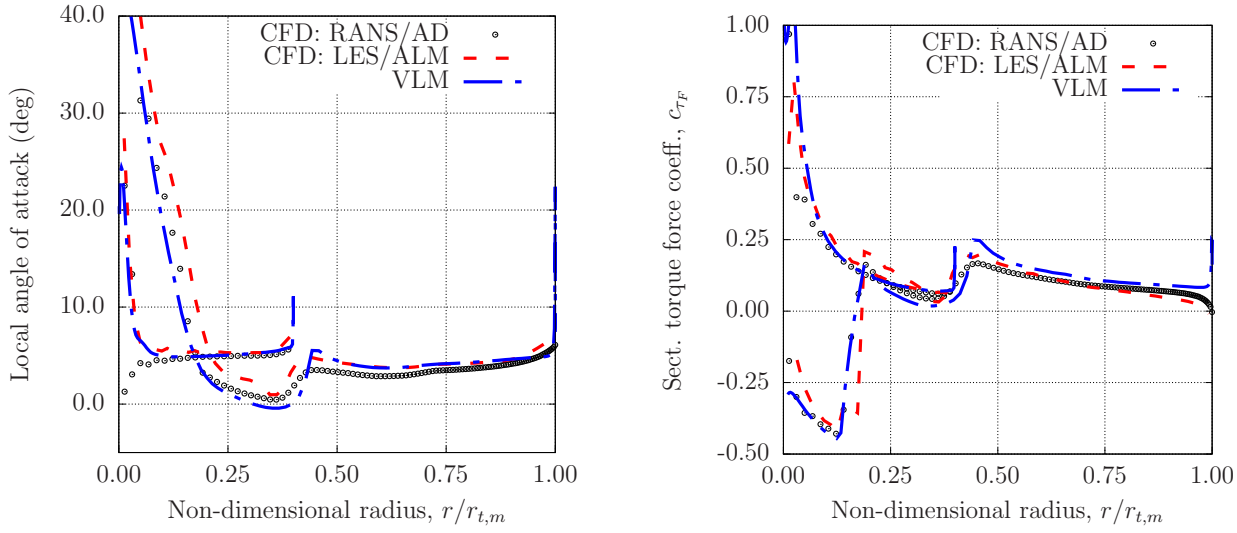

(a) angle of attack, α

(b) sectional torque force coeff., $c_{\tau F}$

Fig. 13: Comparisons between CFD and VLM of spanwise variations of angle of attack and torque force coefficient for the following parameters of the secondary rotor: $r_{t,s}/r_{t,m} = 0.40$ and $\lambda_s = 8.0$.

tip speed ratio, and rotor-rotor separation were varied. In this paper, we focus on varying only two parameters: rotor-rotor separation and secondary rotor tip speed ratio.

Figure 14 compares the results of parametric sweeps performed using the RANS/AD method and the vortex lattice method described in the previous sections. While the overall magnitudes are not predicted exactly, a good qualitative agreement is observed between the RANS/AD predictions and the VLM predictions of C_P enhancement with DRWTs. Both the methods suggest maximum gains for a DRWT design with r/r_t between 0.3 and 0.4 and secondary rotor tip speed ratio between $6-10$. This verifies the ability of the proposed prescribed wake vortex lattice method to carry out preliminary design/analysis of dual-rotor wind turbines. The vortex lattice method is significantly inexpensive compared to the RANS/AD method; its computational cost is two orders of magnitude less than that of the RANS/AD method making it a good choice for preliminary design.

To estimate the aerodynamic performance improvement offered by the DRWT concept over a range of turbine operating conditions, a secondary rotor design with rotor-rotor separation of $0.25 \times r_{t,m}$, $r_{t,s}/r_{t,m} = 0.4$ and $\lambda_s = 8$ is selected. A sweep of main rotor tip speed ratio is performed (while keeping λ_s fixed) with the proposed VLM and the results are compared against SRWT in Fig. 15. The DRWT offers enhanced energy capture for $\lambda_m \leq 7.5$. At higher λ_m, the secondary rotor gives a performance penalty. This performance penalty is due to non-optimal choice of λ_s, which can be avoided by identifying the right combinations of λ_m and λ_s to use during turbine operation. Similarly, the enhanced performance of the DRWT for $\lambda_m \leq 7.5$ may further improve by varying λ_s with λ_m.

5 Conclusion

A prescribed wake vortex lattice method (VLM) to perform preliminary aerodynamic analysis of dual-rotor wind turbines is proposed. Modifications from previous works in the description of the trailing vortex helix are described. The method is validated against experimental data and blade element momentum (BEM) theory results for a conventional, single-rotor wind turbine. The agreement between the measured and predicted power curves is good away from stall. The agreement between the VLM and BEM predictions for sectional torque and thrust force distributions is very good. The method is extended to analyze dual-rotor wind turbines by assuming pseudo-steady flow and averaging results

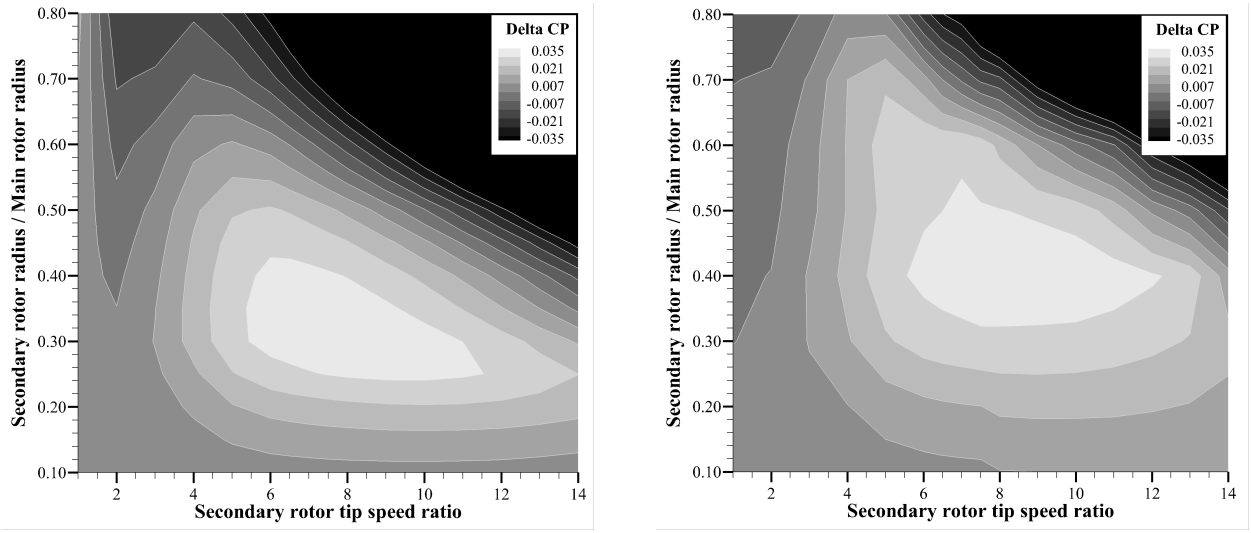

(a) RANS (b) VLM

Fig. 14: Parametric sweep results - contours of difference in aerodynamic power coefficient, $\Delta C_P = C_{P\text{DRWT}} - C_{P\text{SRWT}}$ as predicted by (a) RANS and (b) VLM are shown. The parameters are tip radius and tip speed ratio of the secondary rotor.

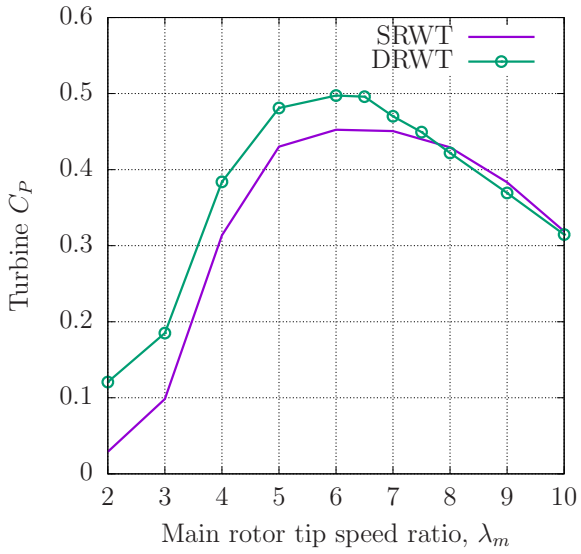

Fig. 15: VLM predictions of aerodynamic power coefficients of a DRWT and the corresponding SRWT as a function of the man rotor tip speed ratio, λ_m.

over multiple relative rotor clock positions. The trailing wake structure of a DRWT is determined by recognizing that the trailing vortices of both rotors of a DRWT convect with the same flow velocity. Singularities in Biot-Savart's formula are avoided by enforcing a minimum threshold on spacing between vortex element center and the point where induction is calculated. Comparisons made with RANS/AD CFD simulations (where the turbine rotors are modeled as actuator disks) and with LES/ALM simulations (where the actuator line model is used to represent rotor blades) show good agreement in predicted spanwise profiles of torque force coefficient and angle of attack.

Parametric sweeps, varying the secondary rotor radius and tip speed ratio are carried out using the proposed VLM and compared with RANS/AD predictions. Both solvers provide similar design

guidance (pointing to similar optimal configuration), proving that the proposed prescribed-wake vortex lattice method can be used as an alternative, inexpensive method to perform preliminary design of DRWTs. Two directions of future research will be explored: (1) develop an inverse design methodology for DRWTs using the VLM developed here, and (2) a full optimization study to explore DRWT designs that minimize wake loss in addition to enhancing isolated turbine performance.

6 Acknowledgment

Funding for this research was provided by the National Science Foundation (Grant #NSF/CBET-1438099), the Iowa Energy Center (Grant #14-008-OG), and the Iowa Space Grants Consortium (Grant #475-20-5). Computational resources used for this research were provided by NSF XSEDE (Grant #TG-CTS130004).

References

[1] Rosenberg, A., Selvaraj, S., and Sharma, A., 2014. "A novel dual-rotor turbine for increased wind energy capture". *Journal of Physics: Conference Series,* ***524***(1).

[2] Moghadassian, B., Rosenberg, A., Hu, H., and Sharma, A., 2016. "Numerical investigation of aerodynamic performance and loads of a novel dual rotor wind turbine". *Energies* **9**(7), 571.

[3] Hu, H., Wang, Z., Ozbay, A., Tian, W., and Sharma, A., 2015. "An experimental investigation on the wake characteristics behind a novel twin-rotor wind turbine". In AIAA Science and Technology Forum and Exposition (SciTech2015).

[4] Jung, S. N., No, T. S., and Ryu, K. W., 2005. "Aerodynamic performance prediction of a 30kw counter-rotating wind turbine system". *Renewable Energy,* ***30***(5), pp. 631–644.

[5] Ozbay, A., Tian, W., and Hu, H., 2014. "An experimental investigation on the aeromechanics and near wake characteristics of dual-rotor wind turbines (drwts)". In AIAA Science and Technology Forum and Exposition (SciTech2014).

[6] Lee, S., Kim, H., Son, E., and Lee, S., 2012. "Effects of design parameters on aerodynamic performance of a counter-rotating wind turbine". *Renewable Energy,* ***42***, pp. 140–144.

[7] Lee, S., Kim, H., and Lee, S., 2010. "Analysis of aerodynamic characteristics on a counter-rotating wind turbine". *Current Applied Physics,* ***10***(2), pp. S339–S342.

[8] Lee, S., Son, E., and Lee, S., 2013. "Velocity interference in the rear rotor of a counter-rotating wind turbine". *Renewable Energy,* ***54***, pp. 235–240.

[9] Kocurek, D., 1987. Lifting surface performance analysis for horizontal wind axis turbines. Tech. Rep. SERI/STR-217-3163; DE87001176, Solar Energy Research Institute, Computational Methodology Associates, 2900 Steve Drive, Hurst, Texas, USA.

[10] Chattot, J.-J., 2002. "Design and analysis of wind turbines using helicoidal vortex model". *Computational Fluid Dynamics Journal,* ***11***(1), pp. 50–54.

[11] Leishman, J. G., 2011. "Aerodynamics of horizontal axis wind turbines". In *Advances in Wind Energy Conversion Technology*. Springer, pp. 1–69.

[12] Chattot, J.-J., 2002. "Optimization of propellers using helicoidal vortex model". *Computational Fluid Dynamics Journal,* ***10***(4), pp. 429–438.

[13] Chattot, J.-J., 2011. "Wind turbine aerodynamics: analysis and design". *International Journal of Aerodynamics,* ***1***(3), pp. 404–444.

[14] Buhl, M., 2005. A new empirical relationship between thrust coefficient and induction factor for the turbulent windmill state. Tech. Rep. NREL/TP-500-36834, National Renewable Energy Laboratory, Boulder, Colorado, USA.

[15] Thelen, A., Leifsson, L., Sharma, A., and Koziel, S., 2016. "Direct and surrogate-based optimization of dual-rotor wind turbines". In 34th Wind Energy Symposium (SciTech 2016).

[16] Schepers, J., Brand, A., Bruining, A., Graham, J., Hand, M., Infield, D., Madsen, H., Paynter, R., and Simms, D., 1997. Final report of iea annex xiv: Field rotor aerodynamics. Tech. Rep. ECN-C-97-027, Energy Research Center of the Netherlands.

[17] Selvaraj, S., 2014. "Numerical investigation of wind turbine and wind farm aerodynamics". Master's thesis, Iowa State University.

[18] Churchfield, M. J., Lee, S., Michalakes, J., and Moriarty, P. J., 2012. "A numerical study of the effects of atmospheric and wake turbulence on wind turbine dynamics". *Journal of Turbulence,* ***13***(14), pp. 1–32.

[19] Launder, B., and Sharma, B., 1974. "Application of the energy-dissipation model of turbulence to the calculation of flow near a spinning disc". *Letters in heat and mass transfer,* ***1***(2), pp. 131–137.

[20] Selvaraj, S., and Sharma, A., 2014. "On predicting the phenomenon of surface flow convergence in wind farms". In ASME Turbo Expo, Paper No. GT2014-25307, American Society of Mechanical Engineers.

[21] Mikkelsen, R., 2003. "Actuator disk models applied to wind turbines". PhD thesis, Technical University of Denmark.